ZnO-based materials and enzymes hybrid systems as highly efficient catalysts for recalcitrant pollutants abatement

ZnO-based materials and enzymes hybrid systems as highly efficient catalysts for recalcitrant pollutants abatement

Marco Sarro [(1)], Nonjabulo P. Gule [(2)], Enzo Laurenti [(1)], Roberta Gamberini [(3)], Maria Cristina Paganini [(1)], Peter E. Mallon [(2)], Paola Calza [(1,*)]

(1) Department of Chemistry, Università di Torino, Via P. Giuria 7, 10125 Torino, Italy

(2) University of Stellenbosch, Department of Chemistry and Polymer Science, Stellenbosch, South Africa

(3) ACEA Pinerolese Company, Corso della Costituzione, 19 - 10064 Pinerolo (TO), Italy

*corresponding author: paola.calza@unito.it

Abstract

The presence of pollutants in water systems is a universal threat. In this study, ZnO based materials and enzyme hybrid materials were evaluated for their ability to remove six emerging waste water pollutants (namely diclofenac, naproxen, iopamidol, imidacloprid, bisphenol A and 2,4-dichlorophenol). These materials were tested in their free form as well as supported on poly(styrene-co-maleic anhydride) (SMA) nanofibre mats fabricated though the process of electrospinning. The SMA nanofibres were fully characterized using Attenuated Total Reflectance-Fourier Transform InfraRed spectroscopy (ATR-FTIR), Thermogravimetric Analysis (TGA), Scanning Electron Microscopy (SEM) and Transmission Electron Microscopy (TEM). Degradation profiles of the activity of these and the Ce-doped ZnO materials in their free form showed good removal efficacy of all the contaminants even in a mixed matrix environment

which mimics a real scenario. By combining Soybean peroxidase (SBP) attached to the SMA nanofibres and oxides nanoparticles into the polymer nanofibers, a synergic effect was observed and it was particularly marked for the Ce-doped ZnO in wastewater treatment. Supporting these materials on the SMA nanofibre mats did not compromise on the effectiveness of the materials. These supported materials offer a potentially easier and more practical application of the materials in water treatment applications.

Keywords: electrospinning, photocatalysis, ZnO, emerging pollutants, wastewater

Introduction

The need for access to clean water cannot be overstated. The world's most precious resource is under strain. Currently a lot of research is underway to find ways of augmenting water resources and water treatment and reuse is at the forefront of these technologies. In modern treatment plants, chemical-biological treatments are effective in the almost complete degradation of organic matter. However, because of the increasingly presence of recalcitrant pollutants, it is necessary to improve wastewaters treatment technologies to obtain an even higher purification of water [1]. The incorporation of environmentally friendly techniques within the water treatment process is also potentially very lucrative. Among the possible ways of doing this, is the exploitation of Advanced Oxidation Processes (AOPs) coupled with biological treatments [2].

The aim of this current work is the preparation and characterization of new hybrid materials containing both a photocatalyst and an enzyme specially designed for obtaining a stable and efficient system useful for the degradation of organic pollutant in wastewater treatment.

The inclusion of a heterogeneous photocatalysis is a powerful solution for environmental remediation because of the possibility to exploit natural solar light. Amongst the class of photocatalysts, zinc oxide (ZnO) is a suitable, cheap and versatile alternative to the most often used titanium dioxide (TiO_2). Additionally, rare earth ion doping induces an improvement of the photocatalytic efficiency of ZnO [3,4]. In this study, Ce-ZnO prepared via the hydrothermal method was selected for the preparation of hybrid materials coupling enzymes with the aim to enhance the oxidation capability of the system towards polluting substrates. Ce-ZnO obtained through different synthetic strategies (i.e. hydrothermal and microwave synthesis) has already shown promising performances in the abatement of several pollutants as well as an improvement of the photocatalytic activity compared to the pristine ZnO [3, 5, 6].

Soybean peroxidase (SBP) was chosen as the enzyme for this study due to its low selectivity and high resistance to chemical and thermal denaturation [7,8]. SBP is a Fe(III)-heme glycoprotein localized in soybean (*Glycine max*) seed coats, where it is involved in the biosynthesis of cell walls

[9,10]. Thanks to its properties, this enzyme seems to be suitable in biotechnological applications, such as the removal of phenol and phenolic derivatives [9,10] or dye degradation [13,14].

Despite the requirement for the addition of H_2O_2 which is a prerequisite for SBP activation, it has been previously shown that the combined use of SBP with semiconductor oxides can improve the capability of the system with regards to the oxidation of contaminants thanks to some key properties [15,16]. Additionally, the oxides could facilitate the start of the degradation of the compounds by forming transformation products toward which SBP is active. The oxide's ability to form H_2O_2 directly in solution eliminates the need to add chemicals for SBP activation.

To exploit the use of photocatalysts in treatment plants, they should be supported to avoid a filtration step and to allow an efficient re-use. Within this contest, a suitable approach could be the employment of electrospinning for the preparation of ultrafine fibres which are characterized by a very high surface area to volume ratio, which results in a potential high loading capacity of the supported substrates and is suitable for catalytic applications [17, 18]. Polymer fibres are formed during the process of electrospinning from a charged jet of a polymer solution with a suitable viscosity, which is stretched because of the electrostatic repulsion between the charges on the surface. It is therefore possible to obtain fine fibres for different applications by mixing a polymer solution with oxide nanoparticles and/or enzymes.

In the last years, few papers have been published dealing with the formation of fibres based on ZnO and doped ZnO which have been used as photocatalysts, sensors and circuit connectors [19-20].

In the current study, we supported the oxides and SBP on poly(styrene-co-maleic anhydride) (SMA) nanofibre mats fabricated through the electrospinning process for the first time. SMA copolymer is a functional polymer due to the presence of reactive maleic anhydride moiety in its backbone. SMA can be prepared by free radical co-polymerization of styrene and maleic anhydride using 2,2′-azobisisobutyronitrile (AIBN) as an initiator. This copolymer has low toxicity, its production is relatively cost effective and it is completely biocompatible [21]. For these reasons, SMA copolymers have been exploited as surface active agents, microbicides, external dopant, drug

carriers, and excellent sorbents for the removal of heavy metal ions [22,23]. The reactive groups on the surface of SMA make it possible to attach the enzymes thus obtaining hybrid materials [16]. We used the electrospinning technique to prepare polymeric nanofibres with SBP combined with ZnO, Ce-ZnO or TiO_2 P25 (as comparing materials). An example of a similar application was reported by Yan et al. who incorporated ZnO nanoparticles (NPs) in polyacrylonitrile nanofibres and exploit their use for water treatment [24]. In this study, we used the SMA polymer nanofibres to obtain a hybrid supported materials which includes SMA-oxides nanoparticles and attached active enzymes.

All the materials have been fully characterized and their activities evaluated toward the abatement of six emerging contaminants (namely diclofenac, naproxen, iopamidol, imidacloprid, bisphenol A and 2,4-dichlorophenol) both in MilliQ water and wastewater. This was done to study the possible matrix effect and to evaluate the potential applicability of the developed materials for their use in real systems.

Diclofenac is an anti-inflammatory drug and it is a halogenate contaminant included on the watching list of the European Union [25]. Naproxen, also an anti-inflammatory drug, has been detected in several places in European surface water [26]. Iopamidol is an iodinated X-ray contrast agent, which is a recalcitrant pollutant not abated during conventional wastewater treatments [27]. 2,4-Dichlorophenol (2,4-DCP) is a well-known contaminant used to produce herbicides [28] and imidacloprid a broad spectrum widely distributed insecticide [29]. Lastly, bisphenol A is employed to produce plastics and it has some reported carcinogenic estrogen-mimicking properties [30].

2. Materials and methods

2.1. Materials and reagents

Poly(styrene-co-maleic anhydride) (SMA-C) was a commercial grade (Mw = 120 000 g/mol) containing about 26 wt% maleic anhydride (MAnh) moieties as a statistical copolymer obtained

from Polyscope, grade SZ 26 120. Bisphenol A (>99.0%), naproxen sodium (98.0-102.0%), imidacloprid (99.9%), diclofenac sodium salt (99.0%), iopamidol (≥98%), 2,4-dichlorophenol, phosphoric acid (≥85.0%), acetonitrile were purchased by Sigma Aldrich. TiO_2-P25 was purchased by Evonik Industries. Effluent wastewaters were provided by ACEA Pinerolese Company. COD was 35 mg/L and the pH was 6.5±0.1.

SBP (RZ = 2.0) was purchased from Bio-Research Products Inc., Iowa-USA, and used without further purification. All solutions were prepared with ultrapure water Millipore Milli-Q^{TM} (TOC<2 ppb, conductivity≥18 MΩ cm).

2.2. Materials synthesis

ZnO NPs were synthetized by the hydrothermal method as described in our previous paper [3]. The synthesized polymer was dissolved in a DMF/acetone solution with a 1:3 v/v ratio. Oxide nanoparticles (NPs) were dispersed into the polymer solution with a concentration of 10% in weight.

Nanoparticles were coupled with SBP via two methods. In the first method, enzymes were added to the spinning solution at a concentration of 1 mg/mL, while in the second method, named the 'POST' method, fibres, already formed, were immersed into a 1 mg/mL enzyme solution in PBS buffer 20 mM at pH=7.4. In both cases, the protein coupling due to the interactions between the maleic anhydride molecules and the amino groups present on the SBP surface [21] was successful. But, in the 'POST' method, SBP did not undergo the stress of the electrospinning process.

Table 1: Synthetized samples description. Electrospinning conditions: 20 kV voltage, 15 cm tip-collector distance, 0.1 mL/min flow rate, normal room temperature and very low humidity maintained using a dehumidifier.

NAME	**SAMPLE DESCRIPTION**
SMA	Pristine SMA nanofibres
SMA-TiO_2	SMA nanofibres + TiO_2 P25 nanoparticles (10% weight/weight)
SMA-ZnO	SMA nanofibres + ZnO nanoparticles (10% weight/weight)

SMA-Ce-ZnO	SMA nanofibres + ZnO (Ce) nanoparticles (10% weight/weight)
SMA-SBP	SMA nanofibres + SBP added to the electrospinning solution
SMA-TiO_2- SBP	SMA nanofibres + TiO_2 P25 nanoparticles (10% weight/weight) + SBP added to the electrospinning solution
SMA-ZnO- SBP	SMA nanofibres + ZnO nanoparticles (10% weight/weight) + SBP added to the electrospinning solution
SMA-Ce-ZnO-SBP	SMA nanofibres + ZnO (Ce) nanoparticles (10% weight/weight) + SBP added to the solution
SMA-Ce-ZnO- SBP	SMA nanofibres + ZnO (Ce) nanoparticles (10% weight/weight) + SBP added to the solution
SMA-SBP POST	SMA nanofibres + SBP added with the post treatment
SMA-TiO_2-SBP POST	SMA nanofibres + TiO_2 P25 nanoparticles (10% weight/weight) + SBP added with the post treatment
SMA-ZnO- SBP POST	SMA nanofibres + ZnO nanoparticles (10% weight/weight) + SBP added with the post treatment
SMA-Ce-ZnO-SBP POST	SMA nanofibres + ZnO (Ce) nanoparticles (10% weight/weight) + SBP added with the post treatment

2.3. Irradiation procedure

Irradiation experiments were carried out using a Pyrex glass cells containing 5 ml of the target molecules in solution. The concentration of the compounds was 10 mg/L when irradiated separately and 2 mg/L in the mixture, while the photocatalyst concentration was 1000 mg/L. The tests with the supported materials were performed in Petri dishes with 30 ml of solution. When nanofibres were tested, a rectangle with an area of 5.35 cm^2 was used with an average concentration of catalyst of 7.8 mg, calculated considered the weight of the fibres and the amount of nanoparticles determined by the TGA measurements.

Samples were subjected to different irradiation times using a Philips TLK/05 lamp 40 Watt with maximum emission at 360 nm. The pH was measured for all samples before and after the irradiation treatment. In the case of the mixture of contaminants, the initial pH was 5.4 and after the photocatalytic treatment it was determined to be 5.1 ± 0.3.

Experiments with soybean peroxidase in aqueous solution were performed in the dark by using the same protocol and analyzing the solution at different reaction times. The concentrations of SBP and H_2O_2 were 1×10^{-8} M and 1×10^{-4} M, respectively.

2.4. Analytical procedures

The disappearance of analytes was monitored using a Merck-Hitachi liquid chromatographer equipped with a Rheodyne injector L-6200 and L-6200A pumps for high-pressure gradients, L-4200 UV-Vis detector (the detection wavelength was set at 240 nm) and a column LiChrocart RP-C18 (Merck, 12,5 cm x 0,4 cm). Isocratic elution (1 mL/min flow rate) was carried out with 80% of phosphate buffer $1x10^{-2}$ M at pH 2.8 and 20% acetonitrile and retention time was 6.45 min. The detection wavelength was set at 220 nm.

The mixture of analytes was detected by using a gradient elution (1 mL/min flow) with 90% phosphate buffer $1x10^{-2}$ M at pH 2.8 and 10% of acetonitrile 10/100 at 0/35. The retention times were 2.26, 13.51, 23.31, 24.07, 24.68 and 29.38 for iopamidol, imidacloprid, bisphenol A, 2,4-dichlorophenol, naproxen and diclofenac. The detection wavelength was set at 210 nm.

2.5 Materials characterization techniques

Powder X-rays diffraction (XRD) patterns were recorded with a PANalytical PW3040/60 X'Pert PRO MPD using a copper Kα radiation source (0.15418 nm). The intensities were obtained in the 2θ ranges between 20° and 100°. The X'Pert High-Score software was used for data handling.

The surface area measurements were carried out on a Micromeritics ASAP 2020 using the Brunauer–Emmett–Teller (B.E.T.) model to analyze the N_2 adsorption isotherms measured at 77K. Prior to each run, all the samples were degassed at 160°C for 3h.

Morphological analysis of the synthesized materials was carried out using scanning electron microscopy (SEM). The SEM is a FEI Nova NanoSEM 230 with a field emission gun (FEG). The samples were carbon coated lightly prior to image acquisition. The beam conditions during the image analysis were 5 kV acceleration voltage Extra-High Tension (EHT) target, 250 pA beam current (I-Probe), less than 4 mm working distance (WD) and a high resolution column configuration (Column Mode). For cross-sectional SEM imaging, the samples were frozen using liquid nitrogen and broken using tweezers prior to coating and imaging the cross sections.

The diameter of the nanofibres was measured using AxioVision at 100 different points and the diameter distribution was plotted to obtain the average diameter of the fabricated mats.

Transmission electron microscopy (TEM) was used for in-depth imaging of the fabricated nanofibres. The TEM used for imaging was a FEI Tecnai T20 equipped with a LaB6 emitter, operating at 200 kV and fitted with a Gatan Tridiem GIF with a 2kX2k CCD camera. Images were collected using Gatan Digital Micrograph software.

Thermogravimetric analysis of the materials was performed on a Q500 thermogravimetric analyzer in air at 10 °C. min^{-1} to determine their thermal stability. This instrument determines changes in weight in relation to change in temperature, which translates to the ability of the material to withstand high temperatures. Weight loss in % was used over the temperature range 0-900 °C.

ATR-FTIR spectroscopy was carried out on a Nexus infrared spectrometer that was equipped with a smart golden gate attenuated total reflectance diamond from Thermo Nicolet with ZnSe lenses. Every sample was scanned 64 times with 4.0 cm-1 resolution. The software that was used on the system to do the data analysis was Omnic Software, version 7.2.

3. Results

3.1. Materials characterization

The S_{BET} analysis of the ZnO and Ce-ZnO samples shows a very low value for the surface area, less than 10 m^2/g as already described elsewhere [3].

The XRD patterns of the samples investigated in this work are shown in the supplemental information (Figure S1). The peaks corresponding to the diffraction patterns of hexagonal Wurtzite phase of ZnO were observed. The introduction of Cerium does not bring about any modifications in the crystal structure of the ZnO, but the cerium introduced as a dopant in the sample generates a new phase of CeO_2 as it can be seen in Figure S1 [3].

In addition to the evaluation of the free compounds, the synthetized oxides and SBP were supported on SMA nanofibres obtained by the electrospinning technique. Hybrid materials prepared with oxides, enzyme and SMA nanofibres were synthetized as described in Table 1, and characterized *via* FTIR, SEM, TEM, TGA and XRD analyses.

Figure 1 shows the ATR-FTIR spectrum of pristine SMA. The absorption bands at 1855 and 1770 cm^{-1} are characteristic for asymmetric and symmetric C=O stretching vibrations from the anhydride groups, while the signals at 1605 cm^{-1} and 1500 cm^{-1} are caused by (C=C) stretching of the aromatic ring and (C–H) bending vibration of the aromatic ring. Bands at 916, 1078 and 1220 cm^{-1} are due to cyclic anhydride groups.

The presence of nanoparticles inside the electrospinning solution could influence the process, due to the changing in the solution properties (i.e. viscosity, charge and surface tension) [32,33]. This is illustrated by the fact that the fibre diameters are different in the presence of the NPs.

Figure 2 shows the nanofibres obtained by coupling the oxides with the SBP enzyme to the oxide containing SMA following two methods (see section 2.2 for details). Details about the Figure 2 are shown in Table 2.

Table 2: Descriptions of images in Figure 2

Figure	Sample description
A1	SEM image of pristine (pure) SMA nanofibres
A2	TEM image of pristine (pure) SMA nanofibres
A3	Cross-sectional SEM image of pristine (pure) SMA nanofibres
B1	SEM image of of SMA-Ce-ZnO nanofibres
B2	TEM image of SMA-Ce-ZnO nanofibres
B3	Cross-sectional SEM image of SMA-Ce-ZnO nanofibres
C1	SEM image of SMA-Ce-ZnO-SBP nanofibres
C2	TEM image of SMA-Ce-ZnO-SBP nanofibres
C3	Cross-sectional SEM image of SMA-Ce-ZnO-SBP nanofibres
D1	SEM image of SMA-Ce-ZnO-SBP (POST) nanofibres
D2	TEM image of SMA-Ce-ZnO-SBP (POST) nanofibres
D3	Cross-sectional SEM image of SMA-Ce-ZnO-SBP (POST) nanofibres

From the SEM images reported in Figure 2 several observations are notable: firstly, the smooth morphology of SMA observed (Figures 2A1-A3) disappears with the addition of Ce-ZnO which is evidenced by the lumpy protrusions in both the SEM (Figure 2B1) and cross-sectional SEM (Figure 2B3) images. The TEM image (Figure 2B2) further confirms the presence of the nanoparticles with the distinct black dots on the nanofibres. With the addition of the SBP enzyme, another distinct morphological change is observed: the nanofibres show some swelling as well as squashing (Figure 2C1-C3). The addition of the peroxidase did not influence the spinnability or the distribution of the nanoparticles inside the nanofibres. Further swelling of the nanofibers is also observed in the images of SMA-Ce-ZnO-SBP (POST) nanofibres (Figures 2D3). Despite all these morphological changes however, the nanofibres maintain their integrity. This is a very important tool considering that the final goal of this work is the use and application of the nanofibres. The diameter variations of the nanofibres were confirmed using diameter measurements taken using

AxioVision software. Figure 3 shows the average distribution of SMA nanofibres and SMA-Ce-ZnO-SBP (POST) nanofibres. The increase from an average of about 200 nm to about 300 nm in diameter was observed on the nanofibre diameters.

The amount of nanoparticles in the composites was determined by TGA analysis as shown in Figure 4. For pristine SMA sample, the total weight loss was about 97%. From 400 K to 450 K it exhibits a weight loss of about 85%, attributable to the decomposition of the polymer. From 450 K to 800 K there is a further weight loss of about 10-12%, due to the decomposition of the remaining organic compounds. The composite materials show a lower total weight loss, due to the presence of nanoparticles, which are thermally stable in this temperature range. The amount of nanoparticles inside the fibres was determined to be 10-15%. Even following the enzyme addition to the materials, the TGA curves show a similar trend as was shown for the Ce-ZnO based materials.

3.2. Evaluation performed in dispersed aqueous matter

Preliminarly, an adsorption test in the dark was done for all the pollutants and, in all cases, it was found to be negligible. The six different pollutants (separately or in mixture) were then treated with the synthetized materials or SBP enzyme dispersed in aqueous solution.

The photocatalytic efficiency of the pristine and cerium doped ZnO (Ce-ZnO) in the abatement of the single compounds in MilliQ water was firstly evaluated and the results are compared with those obtained with the benchmark, TiO_2. It was found that the Ce-ZnO led to the fastest degradation of all compounds, as shown in Figure 5. The high efficiency of the Ce-ZnO was remarkable toward all pollutants and, in particular, on the degradation of iopamidol, the most recalcitrant compound. This is in agreement with data already reported by some of us [3]. In the presence of the Ce-ZnO sample, iopamidol was almost completely degraded within 15 minutes. At that time, only 35% was abated using TiO_2 as catalyst. Naproxen exhibits the fastest degradation with all materials tested

and a complete abatement was obtained within 15, 13 and 7 min in the presence of TiO_2, pristine ZnO and Ce-ZnO, respectively.

The same experiments were repeated in the presence of the SBP 1×10^{-8} M and hydrogen peroxide 2×10^{-4} M. SBP led to the complete removal of 2,4-DCP and bisphenol A within 20 and 70 min, respectively, and to a partial degradation of the other organic compounds. After 2h, 20% of the naproxen and diclofenac, 12% of the imidacloprid, and 4% of the iopamidol were degraded (Figure 6).

The photocatalytic efficiency of the materials was then tested toward the abatement of a mixture of the six contaminants in MilliQ water and effluent wastewater (EWW). Figure 7 shows abatement curves for each pollutant. The pseudo-first order kinetic constants were determined and are shown in Table 3. Once again, the Ce-ZnO led to the fastest abatement of all pollutants in both matrices and the kinetic improvement was remarkable above all toward the abatement of iopamidol, bisphenol A and 2,4-dichlorophenol. In MilliQ water, the kinetic constant values increased nearly four times for iopamidol and imidacloprid and three times for 2,4-dichlorophenol when passing from TiO_2 to Ce-ZnO. With TiO_2 the time of abatement increased from 10 min for diclofenac and naproxen up to more than 20 minutes for iopamidol, imidacloprid and 2,4-DCP (see Figure 7A, left). In the case of the naproxen, the fastest abatement was achieved in the presence of Ce-ZnO, where 4 minutes were enough to achieve its complete degradation, while 10 or 12 min were required for TiO_2 and pristine ZnO, respectively.

Table 3: Kinetics constants for the abatement of the contaminants in MilliQ water and effluent wastewater with TiO_2, ZnO, Ce-ZnO and SBP.

k, x10^2(min^{-1})	**Matrix**	**2,4-DCP**	**IMIDACLOPRID**	**IOPAMIDOL**	**NAPROXEN**	**BISPHENOL-A**	**DICLOFENAC**
TiO_2	**MilliQ**	8.30	4.90	4.10	39.1	21.2	31.0

	EWW	3.50	1.80	1.50	4.20	3.60	4.10
ZnO	**MilliQ**	6.10	5.40	3.20	28.5	14.8	22.5
	EWW	5.9	5.30	1.80	15.5	10.9	14.8
Ce-ZnO	**MilliQ**	30.2	19.00	15.50	76.3	45.2	52.9
	EWW	10.0	9.10	2.30	31.1	16.2	26.7
SBP	**MilliQ**	11.4	0.10	0.05	0.30	3.40	0.50
	EWW	6.30	0.07	0.02	0.20	2.00	0.40

In EWW, a loss of efficiency occurred for all the photocatalysts, but the Ce-ZnO still maintained the highest activity toward the abatement of all the investigated compounds even in the presence of the potential interferences (like the dissolved organic matter and inorganic ions in wastewater). In the presence of TiO_2, only diclofenac and naproxen were almost completely degraded within 60 min, while with the Ce-ZnO all compounds were completely abated in the same time window, with iopamidol as the only exception (Figure 7C, right). When analyzing the kinetic constant values for the naproxen, diclofenac and imidacloprid the kinetic constants were seven, six and five times higher respectively with the Ce-ZnO than in the case of the TiO_2.

Experiments with the SBP in aqueous solution confirm the good capability of peroxidases in degradation of 2,4-DCP and bisphenol A [26], whereas the abatement of the other compounds is much slower. Comparing the kinetic constant values obtained in the two matrices, the decrease in the wastewater is marked only in the case of 2,4-DCP and bisphenol A (almost two times lower), while it is less noticeable for diclofenac, iopamidol, imidacloprid and naproxen. It is possible to hypothesize that the photocatalytic activity of semiconductors is negatively influenced by the presence of dissolved organic matter inside the wastewater, which could act as scavenger of radical intermediates, whereas the enzyme activity is less influenced by the presence of the same species.

During the photocatalytic process, a large number of highly reactive radicals, such as superoxide anions and hydroxyl radicals, are generated. The reaction between them can led to the formation of H_2O_2 following the process (Eq. 1-3):

$O_2^{-\bullet} + {}^{\bullet}OH \rightarrow HOO^{\bullet}$ Eq.1

$HOO^{\bullet} + e^{-} \rightarrow HOO^{-}$ Eq.2

$HOO^{-} + H^{+} \rightarrow H_2O_2$ Eq.3

As previously observed in systems with the contemporary presence of TiO_2 and SBP [15, 16], the generated H_2O_2 can activate the catalytic cycle of SBP and contribute to the oxidative process. Moreover, intermediate species formed by photocatalysis can be also oxidized by SBP, increasing the overall degradation rate.

Measurements of the production of H_2O_2 were performed for all oxides (Figure S2) and they showed that the Ce-ZnO lead to the most efficient production of H_2O_2. According to these results the combination between Ce-ZnO and SBP is expected to improve the oxidation capability of the combined system.

3.3. Photo-activity test of the self-supported materials

The performance of nanofibres activity was tested on the mixture of the six contaminants. The absorption on fibres performed in the dark showed negligible results (Figure S3). The fibres with SBP attached showed a weak activity when H_2O_2 ($1x10^{-4}$ M) was added to the solution, as shown in Figure S4.

The photoactivity was once again tested in two matrices, MilliQ water and EWW, and the calculated kinetic constants determined are shown in Table 4. The results show that the efficacy of the nanofiber composite materials was maintained relative to the free materials. This is due to the extremely high surface area of the materials. The Ce-doped ZnO materials once again maintained the best performance when dispersed in nanofibres. As previously described in a recent paper by some of us [rif], the role of Cerium in zinc oxide is crucial in the formation of interfaces that seem

to be the active site during the irradiation process. In MilliQ water, SMA-TiO_2 and SMA-ZnO exhibited scarce abatement of the contaminants, with only the 2,4-DCP being the exception. This compound was almost completely degraded in 24 hours. When analyzing the data for the hybrid materials, it is evident that there is a synergic effect between the oxide and enzyme in almost all the cases. It is evident from the results that the best performances are obtained for the nanofibres prepared through the POST attachment method. This is most likely due to the fact that the SBP may undergo a partial denaturation during the electrospinning process, resulting in a decrease in the enzymatic activity. It is notable that the effect of SBP is evident for all the substrates. In the case of the SMA-Ce-ZnO and SBP prepared through the POST method, the kinetic constants for iopamidol, imidacloprid and bisphenol A increased from $2.17x10^{-4}$ min^{-1}, $2x10^{-4}$ min^{-1} and $2x10^{-4}$ min^{-1} (SMA-Ce-ZnO only) to $12x10^{-4}$ min^{-1}, $9.33x10^{-4}$ min^{-1} and $7.17x10^{-4}$ min^{-1} (SMA-Ce-ZnO plus SBP). Once again, the best performance was achieved with the Ce-ZnO composite, which led to the complete abatement of diclofenac and 2,4-DCP, 90% of naproxen, 85% of imidacloprid and 70% of iopamidol and bisphenol A all within 24 h.

Table 4: Kinetic constants calculated for the abatement of the contaminants with the different materials in MilliQ and effluent wastewater (EWW).

k, $x10^5(min^{-1})$	**Matrix**	**2,4-DCP**	**IMIDACLOPRID**	**IOPAMIDOL**	**NAPROXEN**	**BISPHENOL A**	**DICLOFENAC**
SMA-TiO_2	**MilliQ**	93.3	3.33	1.50	30.0	13.3	36.67
	EWW	6.67	6.67	1.00	1.50	15.0	0.13
SMA-ZnO	**MilliQ**	98.33	33.3	-	10.00	20.0	35.0
	EWW	5.00	15.0	3.33	-	13.3	15.00
SMA-Ce-ZnO	**MilliQ**	86.7	20.0	21.67	151.7	20.0	96.67
	EWW	31.7	11.7	6.67	21.67	5.00	18.33

SMA-TiO_2-SBP	**MilliQ**	110	50.0	30.0	51.7	55.0	28.33
	EWW	66.7	6.67	1.67	41.7	30.0	36.67
SMA-ZnO-SBP	**MilliQ**	86.7	6.67	-	11.67	15.0	6.67
	EWW	66.7	3.30	1.67	39.0	11.7	10.6
SMA-Ce-ZnO-SBP	**MilliQ**	117	93.3	73.3	98.3	78.3	50.0
	EWW	108	11. 7	23.3	40.0	31.67	18.3
SMA-TiO_2-SBP POST	**MilliQ**	86.7	5.00	23.3	45.0	5.00	26.7
	EWW	167	6.67	13.3	50.0	23.3	10.0
SMA-ZnO-SBP POST	**MilliQ**	157	10.00	6.67	41.7	43.3	30.00
	EWW	142	11.7	6.67	38.3	35.0	23.33
SMA-Ce-ZnO-SBP POST	**MilliQ**	183	93.3	120	161.7	71.67	163.3
	EWW	130	35.0	50.0	121.7	56.67	61.67

The synergic effect between the oxides and SBP was even more marked in the EWW for all materials. Materials obtained with Ce-ZnO were the most efficient probably thanks to the combination of the higher photocatalytic activity of the oxide comparing to the ZnO and the P25 [3] and to the higher production of H_2O_2 that can activate the SBP. Comparing the SMA-Ce-ZnO composite with the SMA-Ce-ZnO-SBP POST materials, it is evident that the constant rates to 4, 7 and 5 times for 2,4-DCP, iopamidol and naproxen, respectively, when the SBP is attached to the nanofibres (see Table 3). This indicates that the SBP does not lose its activity when dispersed (or attached) to the fibres and that the active role played by SBP is maintained. It has already been shown that this is the case when attached to monoliths [16] or on a polymeric filler [15] in the presence of TiO_2. These results have shown that this activity is still maintained and even enhanced in the electrospun fibres and in the presence of Cerium doped ZnO.

Conclusions

In this paper a great attention was focused on the synthesis, characterization and testing of new type of hybrid materials obtained by supporting semiconductor oxides and SBP onto electrospun nanofibres. The composite nanofibres containing the oxide nanoparticle were produced by electrospinning SMA polymer in the presence of the NPs. The results show that these NPs where successfully incorporated into the polymer nanofibres, both when added to the electrospinning solution and with the POST method.

The ZnO-based materials and enzyme hybrid materials in their free form as well as supported on nanofibres were tested with regards to the efficacy for the removal of several emerging contaminants in wastewater. It was shown that the catalytic activity increased by combining Ce-doped ZnO with SBP for the removal of substrates with different chemicals properties. Moreover, this advantage was maintained when those materials were applied in a complex matrix.

Importantly, the nanofiber composite materials maintained the efficacy respect to the free materials. Moreover, the attached enzyme and the NPs containing nanofibres have a synergic effect, particularly evident in the treatment of the most recalcitrant substrates. It should also be noted that SBP, in the composite materials, significantly enhances the reaction rate even in the case of substrates to which it has a low affinity, thus expanding the application field of this enzyme. Finally, our results show for the first time that even in effluent wastewater, the Ce-doped ZnO photocatalyst, included in the polymer nanofibres and attached with the active enzyme, exhibit a high efficiency and could then be potentially used for the abatement of recalcitrant pollutants in tertiary water treatment. These supported treatment systems potentially increase the applications of self-supported materials to the abatement of pollutants and open the door to real systems.

Acknowledgments

We acknowledge support from a Marie Curie International Research Staff Exchange Scheme Fellowship (MAT4TREAT, proposal no. 645551) within the Horizon 2020 European Community Framework Programme. We acknowledge support by MIUR, in the frame of the collaborative international consortium WATERJPI2013-MOTREM of the "Water Challenges for a Changing World" Joint Programming Initiative (WaterJPI) Pilot Call as well.

References

[1] C. Prasse, D. Stalter, U. Schulte-Oehlmann, J. Oehlmann, T.A. Ternes, Spoilt for choice: a critical review on the chemical and biological assessment of current wastewater treatment technologies, Water Res. 87 (2015) 237-270

[2] I. Oller, S. Malato, J.A. Sánchez-Pérez, Combination of advanced oxidation processes and biological treatments for wastewater decontamination - a review, Sci. Total Environ. 409 (2011) 4141-4166

[3] M.C. Paganini, D. Dalmasso, C. Gionco, V. Polliotto, L. Mantilleri, P. Calza, Beyond TiO_2: Cerium-Doped Zinc Oxide as a New Photocatalyst for the Photodegradation of Persistent Pollutants, ChemistrySelect 1 (2016) 3377-3383

[4] N. Kaneva, A. Bojinova, K. Papazova, D. Dimitrov, Photocatalytic purification of dye contaminated sea water by lanthanide (La^{3+}, Ce^{3+}, Eu^{3+}) modified ZnO, Catal. Today 252 (2015) 113–119

[5] M. Rezaei, A. Habibi-Yangjeh, Simple and large scale refluxing method for preparation of Ce-doped ZnO nanostructures as highly efficient photocatalyst, Appl. Surf. Sci. 265 (2013) 591- 596

[6] M. Rezaei, A.Habibi-Yangjeh, Microwave-assisted preparation of Ce-doped ZnO nanostructures as an efficient photocatalyst, Mater. Lett. 110 (2013) 53-56

[7] J.K.A. Kamal, D.V. Behere, Thermal and conformational stability of seed coat soybean peroxidase, Biochemistry 41 (2002) 9034-9042

[8] B. Boscolo, E. Laurenti, E. Ghibaudi, ESR spectroscopy investigation of the denaturation process of soybean peroxidase induced by guanidine hydrochloride, DMSO or heat, Protein J. 25 (2006) 379-390

[9] J.W. Gillikin, J.S. Graham, Purification and developmental analysis of the major anionic peroxidase from the seed coat of Glycine max, Plant Physiol. 96 (1991) 214-220

[10] K.G. Welinder, Y.B. Larsen, Covalent structure of soybean seed coat peroxidase, Biochi. Biophys. Acta 1689 (2004) 121-126

[11] A. Bassi, G. Zeng, M. Gijzen Enzymatic removal of phenol and chlorophenols using soybean seed hulls Eng. Life. Sci. 4 (2004) 125-130

[12] C. Watanabe, A. Kashiwada, K. Matsuda, K. Yamada, Soybean peroxidase-catalyzed treatment and removal of BPA and bisphenol derivatives from aqueous solutions, Environ. Prog. Sustain. En. 30 (2011) 81-91

[13] T. Marchis, P. Avetta, A. Bianco Prevot, D. Fabbri, G. Viscardi, E. Laurenti, Oxidative degradation of Remazol Turquoise Blue G 133 by soybean peroxidase, J. Inorg. Biochem. 105 (2011) 321-327

[14] M.C. Silva, J.A. Torres, L.R.V. de Sa, P.M.B. Chagas, V.S. Ferreira-Leitao, A.D. Correa, The use of soybean peroxidase in the decolourization of Remazol Brilliant Blue R and toxicological evaluation of its degradation products, J. Mol. Catal. B-Enz. 89 (2013) 122-129

[15] P. Calza, P. Avetta, G. Rubulotta, M. Sangermano, E. Laurenti, TiO_2-soybean peroxidase composite materials as a new photocatalytic system, Chem. Eng J. 239 (2014) 87-92

[16] P. Calza, D. Zacchigna, E. Laurenti, Degradation of orange dyes and carbamazepine by soybean peroxidase immobilized on silica monoliths and titanium dioxide, Environ Sc. Pollut. Res. 23 (2016) 23742-23749

[17] A. Baji, Y.-W. Mai, S.-C. Wong, M. Abtahi, P. Chen, Electrospinning of polymer nanofibers: Effects on oriented morphology, structures and tensile properties, Compos. Sci. Technol. 70 (2010) 703-718

[18] D. Li,Y. N. Xia, Electrospinning of Nanofibers: Reinventing the Wheel?, Adv. Mater. 16 (2004) 1151-1170

[19] G. X. Wan, S. Y. Ma, X. B. Li, F. M. Li, H. Q. Bian, L. P. Zhang, W. Q. Li, Synthesis and acetone sensing properties of Ce-doped ZnO nanofibers, Mater. Lett. 114 (2014) 103-106

[20] G. Cadafalch Gazquez, S. Lei, A. George, H. Gullapalli, B. A. Boukamp, P. M. Ajayan, J. E. Ten Elshof, Low-Cost, Large-Area, Facile, and Rapid Fabrication of Aligned ZnO Nanowire Device Arrays, ACS Appl. Mater. Interfaces 8 (2016), 13466-13471.

[21] W. J. Cloete, C. Adriaanse, P. Swart, B. Klumperman, Facile immobilization of enzymes on electrospun poly (styrene-alt-maleic anhydride) nanofibers, Polym. Chem. 2 (2011) 1479-1481

[22] X. Zhang, H. Li, M. Cao, L. Shi, C. Chen, Adsorption of Basic Dyes on β-Cyclodextrin Functionalized Poly (Styrene-Alt-Maleic Anhydride), Sep. Sci. Technol. 50 (2015), 947–957.

[23] E. Nazarzadeh Zare, M. Mansour Lakouraj, P. Najafi Moghadam, R. Hasanzadeh, Novel conducting nanocomposite based on polypyrrole and modified poly(styrene-alt-maleic anhydride) via emulsion polymerization: Synthesis, Characterization, Antioxidant, and heavy metal sorbent activity, Polym. Compos. 36 (2015) 138–144.

[24] Y. Han, S. K. Obendorf, Reactivity and reusability of immobilized zinc oxide nanoparticles in fibers on methyl parathion decontamination, Text. Res. J. 86 (4) (2016) 339-349.

[25] P. Schröder, B. Helmreich, B. Škrbić, M. Carballa, M. Papa, C. Pastore, Z. Emre, A. Oehmen, A. Langenhoff, M. Molinos, J. Dvarioniene, C. Huber, K. P. Tsagarakis, E. Martinez-Lopez, S. Meric Pagano, C. Vogelsang, G. Mascolo, Status of hormones and painkillers in wastewater effluents across several European states—considerations for the EU watch list concerning estradiols and diclofenac, Environ. Sci. Pollut. R. 13 (2016) 12835-12866

[26] P. Grenni, L. Patrolecco, N. Ademollo, A. Tolomei, A.B. Caracciolo, Degradation of gemfibrozil and naproxen in a river water ecosystem, Microchem. J. 107 (2013) 158–164

[27] D. Fabbri, P. Calza, D. Dalmasso, P. Chiarelli, V. Santoro, C. Medana, Iodinated X-ray contrast agents: Photoinduced transformation and monitoring in surface water, Sci. Total Environ. 572 (2016) 340-351

[28] K. Fytianos, E. Voudrias, E. Kokkalis, Sorption-desorption behaviour of 2,4-dichlorophenol by marine sediments, Chemosphere 4 (2000) 3-6

[29] S. Rossi A. G. Sabatini R. Cenciarini S. Ghini S. Girotti, Use of High-Performance Liquid Chromatography–UV and Gas Chromatography–Mass Spectrometry for Determination of the Imidacloprid Content of Honeybees, Pollen, Paper Filters, Grass, and Flowers, Chromatographia 61 (2005) 189–195

[30] M. Gmurek, M. Olak-Kucharczyk, S. Ledakowick, Photochemical decomposition of endocrine disrupting compounds - A review, Chem. Eng. J. 310 (2017) 437-456

[31] Q. Husain, S. Qayyum, Biological and enzymatic treatment of bisphenol A and other endocrine disrupting compounds: a review, Crit. Rev. Biotechnol. 33 (2013) 260–292

[32] Z.-M. Huang, Y.-Z. Zhang, M. Kotaki, S. Ramakrishn, A review on polymer nanofibers by electrospinning and their applications in nanocomposites, Compos. Sci. Technol. 63 (2003) 2223-2253

[33] S. Sinha Ray, S.-S. Chen, C.-W. Li, N. C. Nguyen, H. T. Nguyen, A comprehensive review: electrospinning technique for fabrication and surface modification of membranes for water treatment application, RSC Adv. 6 (2016) 85495-85514

Figure captions

Figure 1: FT-IR spectrum of pristine SMA.

Figure 2*:* SEM and TEM and cross-sectional SEM images of fabricated materials as described in Table 1

Figure 3: Fibre diameter analysis indicating an increase in fibre diameter from around 200 nm for the pure SMA nanofibres to around 300 nm in the case of SMA-Ce-ZnO-SBP (POST) nanofibres

Figure 4: TGA curves of pristine SMA and SMA-ZnO (Ce) nanofibres functionalized with SBP.

Figure 5: Degradation profiles of the single contaminants (10 mg/l) using TiO_2 (A), pristine ZnO (B), and Ce-doped ZnO (C) in MilliQ water.

Figure 6: Degradation profiles over time for the pollutants (10 mg/l) with SBP (1×10^{-8} M) and H_2O_2 (1×10^{-4} M).

Figure 7: Curves of the abatement of the pollutants mixture (2 mg/l each) in MilliQ water (left) and wastewater (right): TiO_2 (A), pristine ZnO (B), and Ce-ZnO (C).

Figure 1

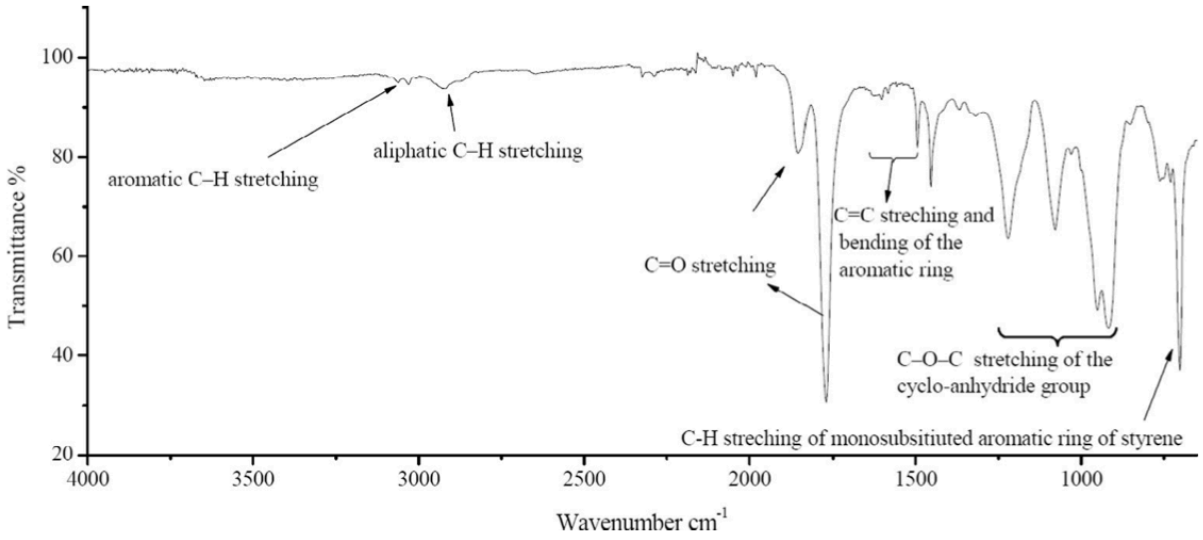
Transmittance %
100
80
60
40
20
4000
3500
3000
2500
2000
1500
1000
Wavenumber cm-1
aromatic C–H stretching
aliphatic C–H stretching
C=O stretching
C=C streching and
bending of the
aromatic ring
C–O–C stretching of the
cyclo-anhydride group
C-H streching of monosubsitiuted aromatic ring of styrene

Figure 2

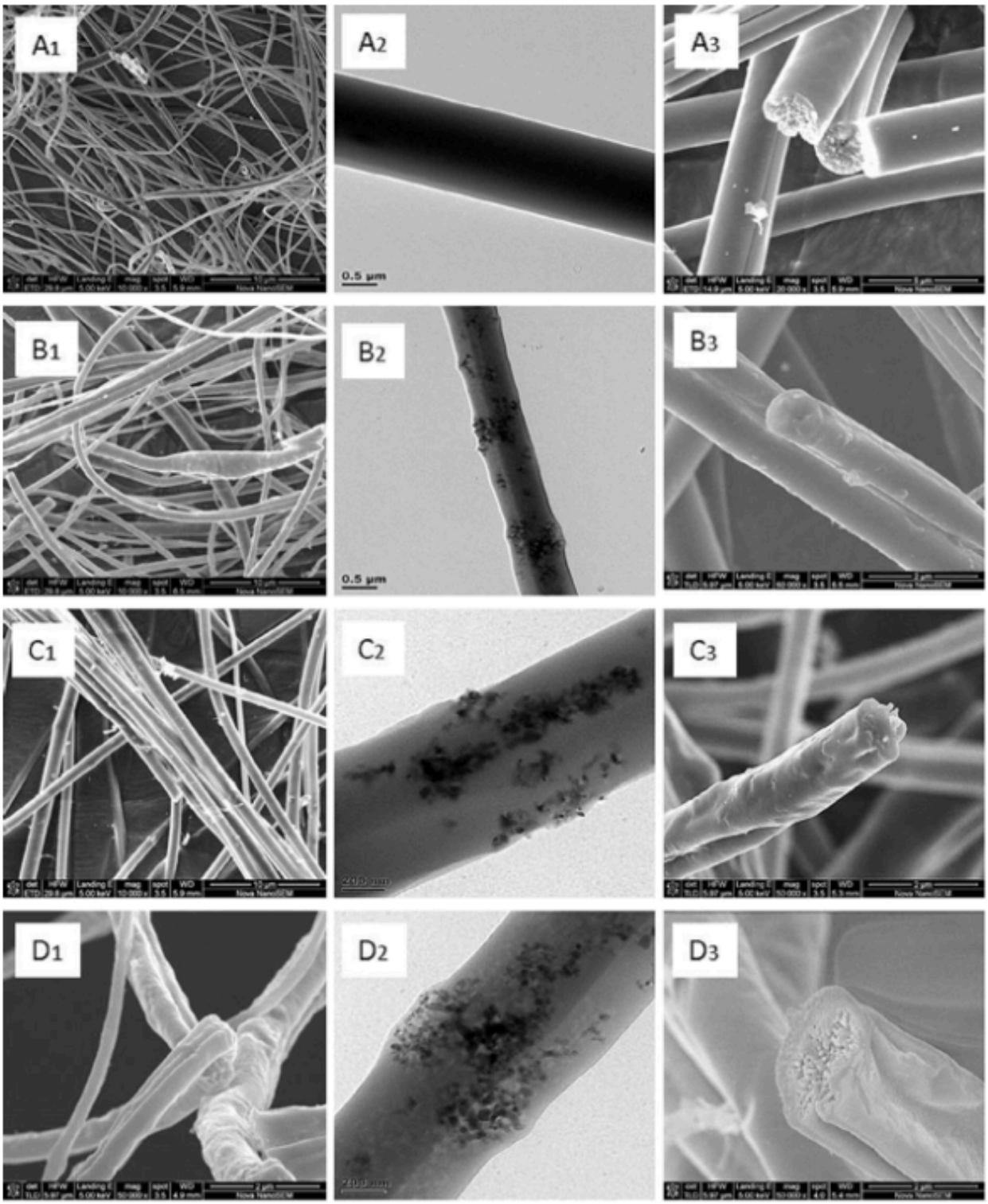

Figure 3

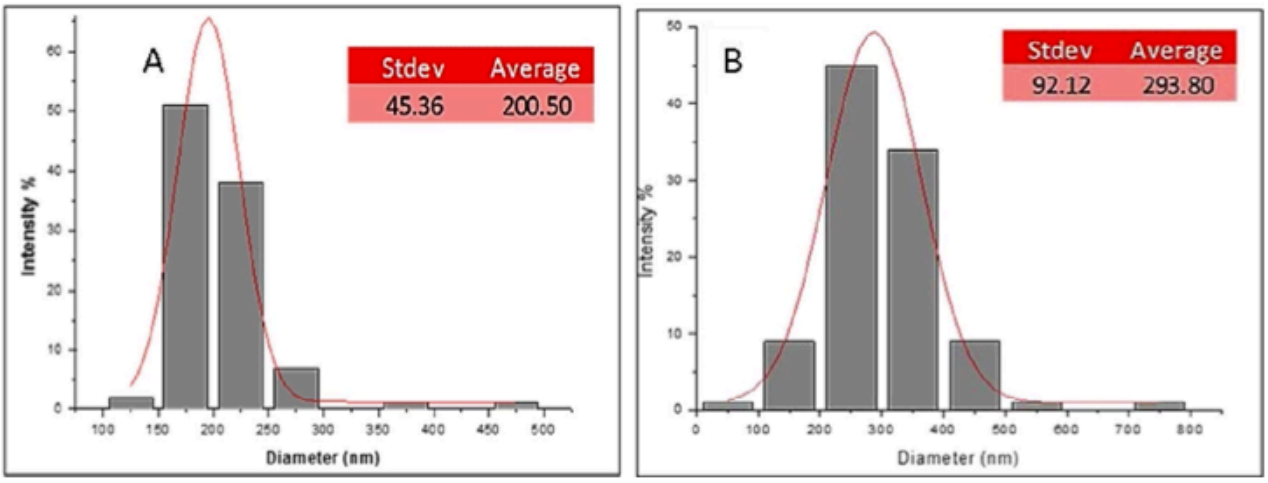

Figure 4

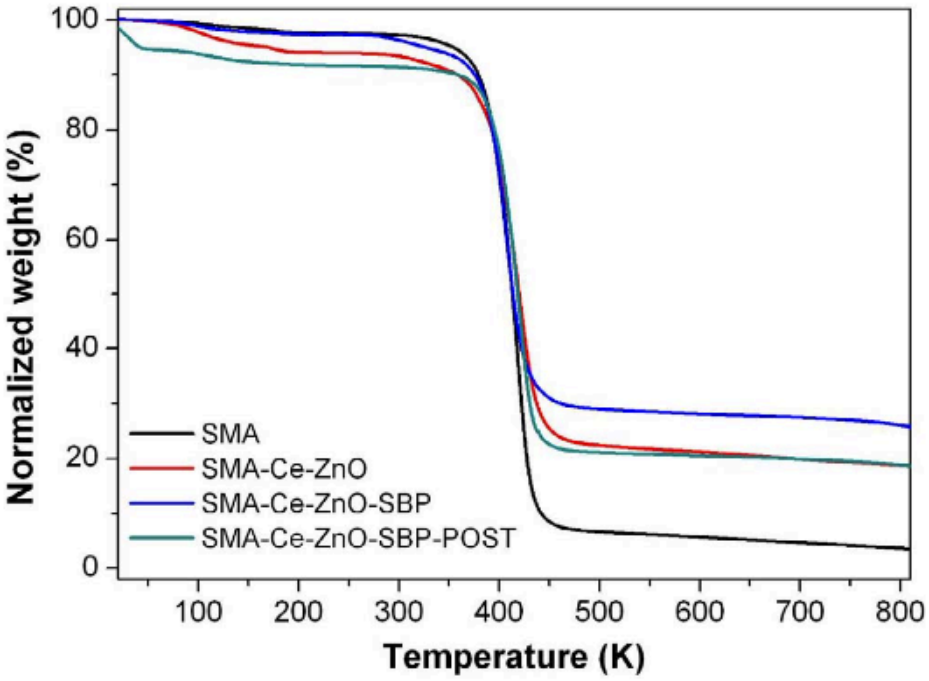

Figure 5

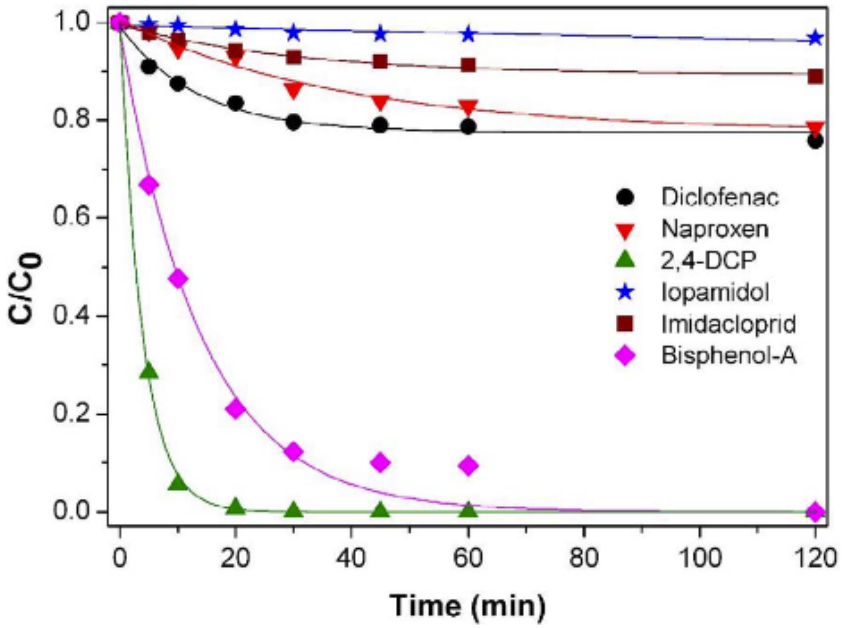
1.0
0.8
0.6
0.4
0.2
0.0
C/C0
0
20
40
60
80
100
120
Time (min)
Diclofenac
Naproxen
2,4-DCP
Iopamidol
Imidacloprid
Bisphenol-A

Figure 6

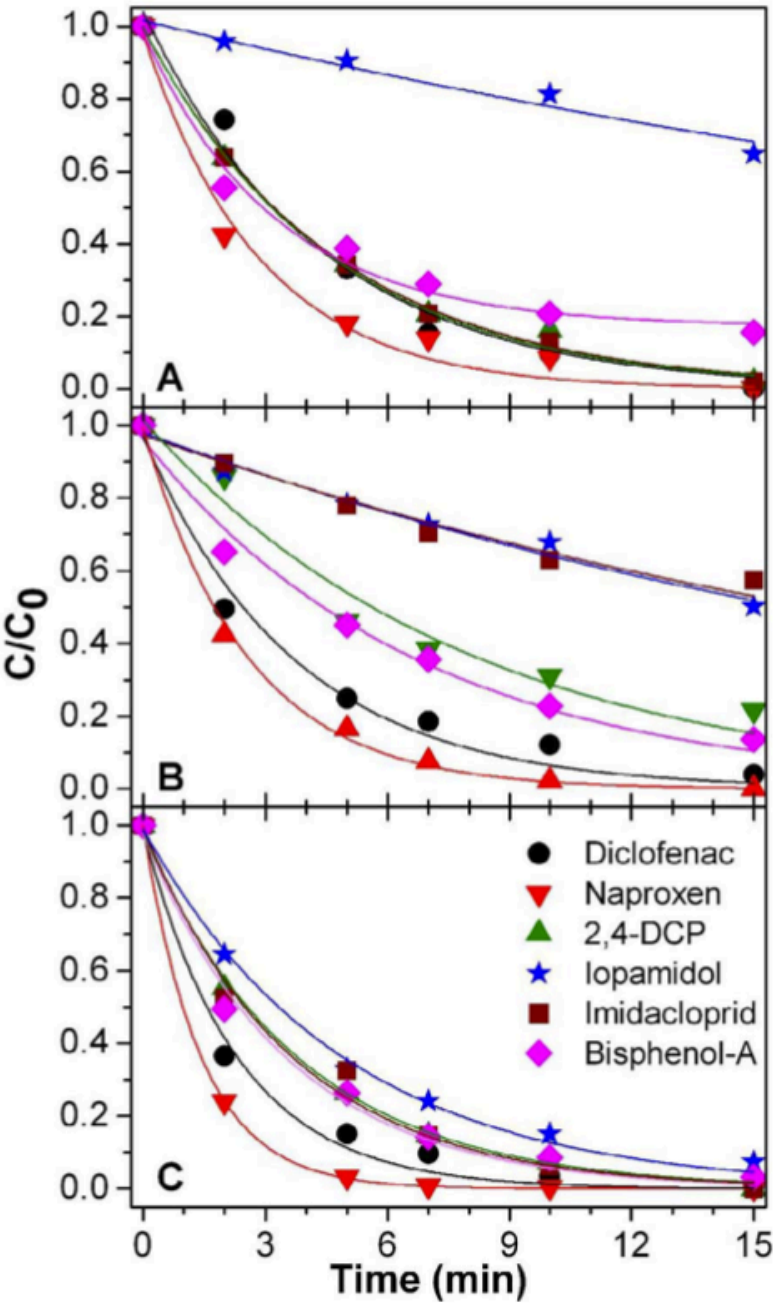
C/C0
Time (min)
A
B
C
Diclofenac
Naproxen
2,4-DCP
Iopamidol
Imidacloprid
Bisphenol-A

Figure 7

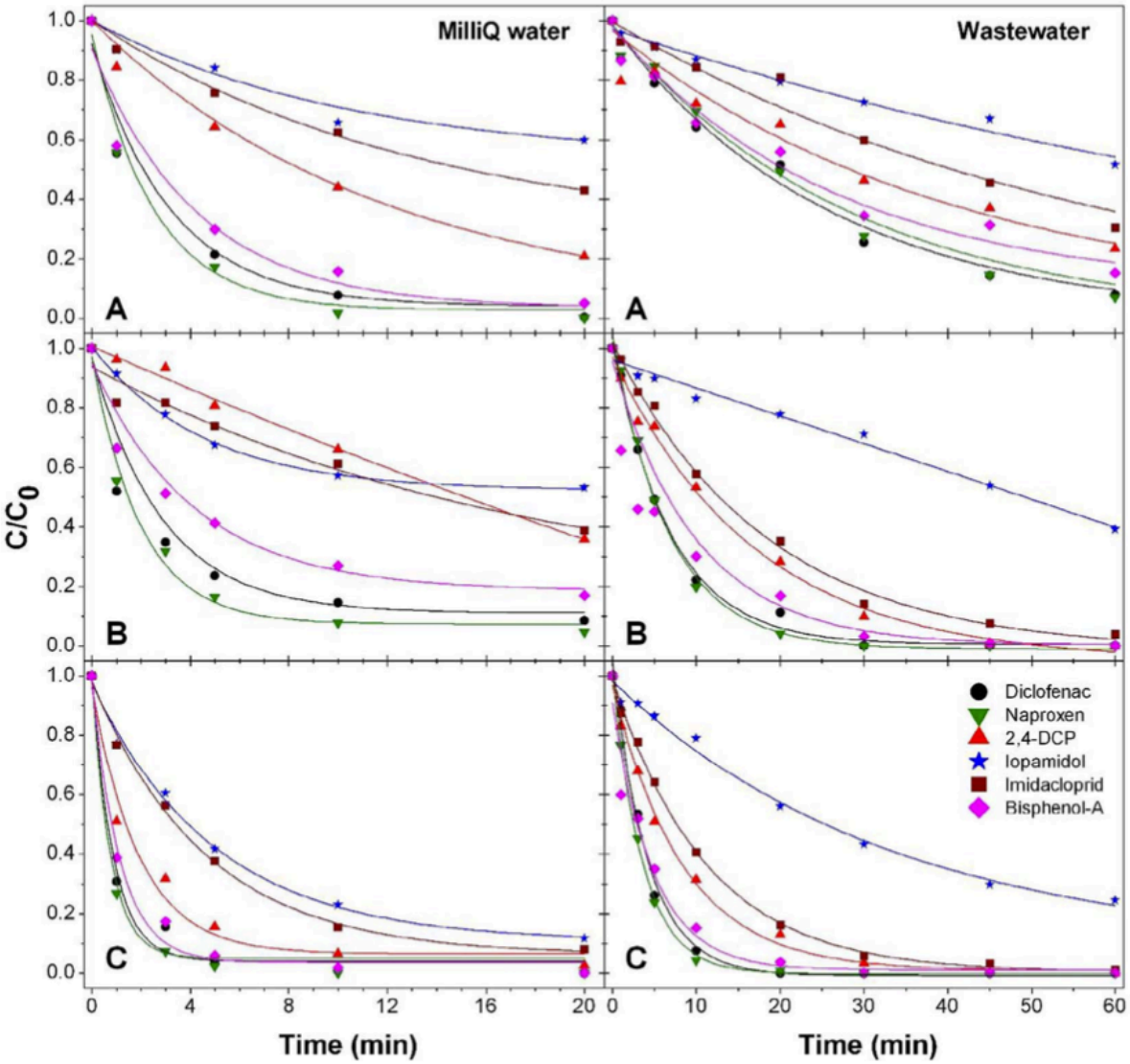
MilliQ water
Wastewater
A
B
C
C/C0
Time (min)
Diclofenac
Naproxen
2,4-DCP
Iopamidol
Imidacloprid
Bisphenol-A